A Framework for Nucleation in Electrochemical Systems and the E
Dendrite Growth

Madison Morey[1], Giacomo Nagaro[4], Anubhab Halder,[3] Sahar Sharifza

[1]Division of Materials Science and Engineering, Boston University, Bos

USA

[2]Department of Mechanical Engineering, Boston University, Boston, M

[3]Department of Electrical and Computer Engineering, Boston Univers

02215, USA

[4]Department of Chemistry, Boston University, Boston, Massachusetts

[5]Department of Physics, Boston University, Boston, Massachusetts 02

*Corresponding author: ryanem@bu.edu, 617-353-7767

Abstract

Dendrite growth is directly attributed to the degradation of battery pe

attributes of dendrite growth have been extensively studied,

computationally, little is understood about the nucleation process ar

and characteristics impact growth. In this study, a numerical mode

the surface energy and improve the stability of the interface leadin
dense and less dendritic. When the defects cause a decrease i
significantly more dendrite growth. Finally, the interplay that surf
properties, due to the composition of the solid-electrolyte interp
dendrite growth is investigated showing that the dominating factor in
growth is improved Li^+ transport through the SEI layer. The results
work can inform approaches to engineering more stable anode-
improved battery performance.

Keywords: Lithium Batteries, Dendrites, Computational Modeling, Nu

1. Introduction:

The energy storage capabilities of state-of-the-art Lithium (Li)-
the low theoretical capacity of the graphite anode (~372 mA h g^{-1})[1].
fall short of society's demand for energy storage technologies in
vehicles and large-scale renewable energy storage[2]. To combat t
battery has emerged as a promising alternative. The Li-metal batte
metal anode which is considered the holy grail of anode technolo

catastrophic failure of the battery[7,8]. A key obstacle in the com

batteries lies in understanding the morphological evolution of de

strategies to control and suppress dendrite growth.

Research into the growth and morphology of Li dendrites has

however, little is known about the nucleation process of Li along th

how surface characteristics, such as surface energy, impact this grow

proposed modes of nucleation such as top and bottom-induced nucl

primarily on defect-induced nucleation where subsurface defects ca

for nucleation or help to stabilize the interface[6]. In particular, the e

in the lattice of Li metal and Li vacancies have on dendrite growth

impurities, like the ones mentioned above, are present in uncycle

example, Li metal films produced via rolling have shown large amou

(O), and Nitrogen (N) impurities[14,15]. Researchers have shown th

decreased using specialized production methods such as thermal eva

be difficult and time-consuming [15]. Therefore, understanding how t

the surface chemistry and in turn, the Li plating can give insight into

transport properties through this layer changed. Liu *et al.*[17] preser
looking at the impact that different components of the SEI layer had
solid-state batteries and in turn the impact it had on Li plating. They
using a Li-11 wt % Sr alloy anode and a fluorinated electrolyte. Then,
experimental characterization, they showed that the interfacial ene
when the SrF_2-rich SEI layer was present as opposed to a bare Li ano
energy combined with changes in the mechanical properties of t
suppression of dendrite growth after cycling.

Additionally, many groups have studied how size, morpholo
impact Li plating for Cu current collectors when initializing the Cu su
batteries (ALMBs) a thin layer of Li is deposited on the Cu current co
For this application, it is crucial that this thin layer is as uniform as p
similar to desiring a Li metal anode that is void of mechanical d
nucleation control methods such as increasing the number of nucleat
using a surface coating that possesses lithophilic cites to control
forming and ensuring that the distribution of nucleates is homogeno

interfaces possessing slower nucleation rates, are more beneficial c
surface area and reduced surface curvature[21–26].

Lopez *et al.*[22] studied how different polymer coatings imp
They found that a low surface energy polymer coating with a high c
reactivity leads to larger Li nucleates, better plating, and improved
cycling. This is because the low surface energy associated with the pol
interaction with the Li metal anode meaning that it did not decre
between the Li metal and polymer resulting in large nucleates wi
minimize the surface area decreasing the reaction flux at the interfac
high interfacial energy results in better plating and overall better ba
al.[23] used a titanium (Ti) metal shield to aid in guided deposition on
shown to have a high interfacial energy providing a higher Li nucleatio
in a low-density distribution of “pancake-like” nucleates and a slow
then showed that the initial morphology of Li nucleates on these sur
through SEM images showing needle-like dendrite growth on a ba
interfacial energy and flat and non-dendritic growth on the high energ

reactive surface area. The morphology of these initial deposits res

growth as opposed to the dendrite growth occurring on the low ener

Researchers have used various methods to model the comp

process on both the atomistic and continuum scales[27–30]. Maeda

Dynamics to study surface nucleation in anorthite-based glass using C

(CNT). Applying this model, they were able to calculate the nucleation

physical parameters. Lu *et al.*[27] developed a transport-based mod

method to aid in the identification of the mechanisms for bubble n

electrodes. Additionally, Jreidini *et al.*[30] uses CNT to calculate liquid

rates and incubation times. They do this using a phase-field crystal m

the gap between the atomic and mesoscale allowing for the consid

subsequent crystal growth. Adopting the techniques that have

applications such as crystal nucleation can provide a starting point

nucleation in alternate systems, such as electrochemical nucleation

[27–30].

Therefore, multiple studies have been proposed to theoretica

charged substrates. Additionally, Monroe and Newman[32] presented (P2D) surface-energy controlled growth model that incorporated curvature into the growth kinetics. The speed at which nucleates f influencing dendrite growth. Nagy *et al.*[33] used computational me parameters including surface energy and overpotential affected the s within a system. They showed that an increase in surface energy lea state nucleation rate because the system has a larger energy to ov Further, it was shown that as the applied potential to the system beca nucleation rate increased.

While the aforementioned theoretical studies were successfu fragments of the nucleation and growth processes, they have se Garcia's[31] analytical framework provided insight into how chara tension and overpotential determined the energetic favorability of de the model only considered the formation and growth process of indiv consider their impact on subsequent dendrite growth. Monroe considered the dendrite tip curvature and surface energy on dendrite

understanding of the impact these parameters and the nucleation

growth and morphology after initial nucleation.

In this paper, we utilize a combination of the theoretical con

to develop a computational model (nucleation-SPH model) that captu

their effects on dendrite growth and morphology by considering

nucleation but also the interfacial transport and the subsequent g

dendrites. This work builds off our previous model that include

electrochemical migration[12], a spatially and temporally varying

extended, concentration-dependent, Butler-Volmer equation that

anode-electrolyte interface[10]. Two main additions have been m

nucleation physics. The first is the addition of a radial growth equati

which a single Li nucleate grows. The second is the addition of a st

equation that tracks how quickly nucleates form in the system with res

including surface energy and overpotential. While many factors imp

including transport properties[36,37], charging methods[9,13], sepa

electrode architecture[10] as studied is past papers utilizing th

dendrite growth. SPH also captures the morphology of the dendrite model is used in conjunction with DFT to study how point defects impurities in the Li-metal anode impact the surface energy and infl anode-electrolyte interface to inform the design of more stable batt the model to consider the interplay of interfacial energy and tra suppression of dendrite growth due to the presence of an LiF-rich SEI

2. Computational Methods:

The model presented in this work solves for species conservati interface and includes the effects of transport of cations thro electrodeposition. The model extends previous electrodeposition mod that surface energy and nucleation have on electrodeposition[10,12 through the addition of a radial growth equation for a single hemisphe state nucleation rate equation derived from Classical Nucleation Theo

The Nernst-Planck equation is solved for the change in co electrolyte, dC/dt, [39]

$$\frac{\partial C_i(\vec{r_f},t)}{\partial t} = \nabla \cdot \left(D_i \nabla C_i(\vec{r_f},t)\right) + z_i \nabla \cdot \left(C_i(\vec{r_f},t) \nabla \phi(\vec{r_f},t)\right)$$

In a binary electrolyte cations and anions remain electr

electrolyte. Upon the application of a voltage, electroneutrality can

diffusion layer due to the consumption of ions at the electrode surfac

violated a charge imbalance occurs and results in an electric pot

gradient can be solved via the electrostatic Poisson equation[39]

$$\nabla^2\phi(\vec{r_f},t) = -\frac{\rho_{charge}}{\epsilon}, \vec{r_f} \in \Omega_f, t > 0$$

the dielectric constant is ϵ, and the net charge density, ρ_{charge}, is giv

$$\rho_{charge} = F\left(z_{M^+}C_{M^+}(\vec{r_f},t) - z_A C_A(\vec{r_f},t)\right)$$

where F is the Faraday constant.

Electrodeposition occurs at the anode-electrolyte interface. D

(M^+) will be reduced via electrons (e^-) and deposit as metal along the

$$M^+ + e^- \rightarrow M$$

through a reactive boundary condition for cations at the anode-elect

$$D_{M^+}\nabla C_{M^+}(\vec{r_s},t) + \mu_{M^+}C_{M^+}(\vec{r_s},t)\nabla\emptyset(\vec{r_s},t) = S_s(\vec{r_s},t),$$

where $\vec{r_s}$ is a location in the solid domain, $S_s(\vec{r_s},t)$ is the total flux

where α_a and α_c are the anodic and cathodic transfer coefficients, res

constant, and T is the temperature. The concentration in the bulk e

for cations and $C_{A,L}$ for anions, k^0 is the reaction rate, $\gamma(\vec{r_s})$ is the su

Li surface and the electrolyte, and V_m is the molar volume. The radius

zero for a perfectly flat surface and $k(\vec{r_s}, t) = 2/r(\vec{r_s}, t)$ for a hem

where $r(\vec{r_s}, t = 0)$ is assumed to be larger than that of the critical ra

stable nucleate, [40–42]

$$r_{eq}^* = \frac{2\gamma(\vec{r_s})V_m}{F|\eta|}$$

The overpotential (η) is given by

$$\eta = \emptyset_{App} - \emptyset_{eq}$$

the equilibrium potential, $\emptyset_{eq}$, is the difference between the local

reference potential and $\emptyset_{App}$ is the potential applied to the system.

The growth rate of the individual nuclei radius, dr/dt, is ca

the Li^+ flux for that nucleate at the anode-electrolyte interface and th

$$\frac{dr}{dt} = S_n(\vec{r_s}, t) * V_m, \qquad \vec{r_s} \epsilon \Gamma$$

where N is the total number of atoms per unit surface area r

$N_A C_{Li^+}(\vec{r_s}, t)d$, N_A is Avogadro's number and d is the thickness of th

the vicinity of the electrode (~10 Å) [33], k_B is the Boltzmann cons

collision of the atoms with the critical nuclei, ω_c, is [33,38]

$$\omega_c = \frac{S_c i_0}{z_{M^+} e}$$

the exchange current density, i_0, is defined by $i_0 = F k^0 C_{M^+,L}^{\alpha_c} C_{A,L}^{\alpha_a}$ [10

ionic species (+1), e is the elementary charge and S_c is the surface are

to the electrolyte, $S_c = 2\pi {r_{eq}^*}^2$. The formation energy of the crit

obtained by[33]

$$\Delta G_c = ze(\eta - \phi_{App})$$

The number of atoms in the critical nucleus, g_c, can be obtain

$$g_c(\vec{r_s}) = \frac{32\pi}{3} \frac{\gamma(\vec{r_s})^3 V_m N_A}{(\eta z F)^3} f(\Theta), \qquad \vec{r_s} \in \Gamma$$

where $f(\Theta) = 1/2 - 3/4\cos(\Theta) + 1/4\cos^3(\Theta)$ is a function of cor

There is a zero-flux boundary condition for the anions at the a

$$D_A(\vec{r})\nabla C_A(\vec{r_s}, t) + \mu_A C_A(\vec{r_s}, t) = 0, \vec{r_s} \in \Gamma$$

The governing equations are implemented into the SPH metho

scheme of Tartakovsky *et al.* for Fickian Diffusion and precipitation[44

of Cannon *et al.* for migration [12], the discretization scheme of Morey

[10] and the heterogenous reaction boundary condition is impler

surface reaction (CSR) method [45]. The final forms of the discretized

below, and further details on their implementations and verifica

references[9–13].

The Nernst-Planck equation (Eq. (1)) is discretized as

$$\frac{DC_{M^+,i}}{Dt} = \sum_{j\in liquid} \frac{2D_{M^+} m_j \overrightarrow{r_{ij}}}{\rho_j \left(\overrightarrow{r_{ij}}\right)^2} \left(C_{M^+,i} - C_{M^+,j}\right) \nabla W$$

$$+ \sum_{j\in liquid} \frac{m_j \overrightarrow{r_{ij}}}{\rho_j \left(\overrightarrow{r_{ij}}\right)^2} \mu_{M^+} \left(C_{M^+,i} - C_{M^+,j}\right) \left(\phi_i - \phi_j\right.$$

$$- S_s \sum_{k\epsilon solid} \frac{m_k}{\rho_k} (\overrightarrow{n_k} + \overrightarrow{n_i})(\beta_k + \beta_i) \nabla W_{ik},\ i \in fl$$

where m, ρ, D and C are the mass, density, diffusion coefficient,

particles respectively. The subscript M^+represents the cations, su

individual SPH fluid particles, and k represents the solid particles. μ

potential. The distance between particles i and j is given by $\overrightarrow{r_{ij}}$, $\vec{n}$ is

characteristic function used to identify the anode interface. S_s is the

$$\frac{DC_{A,i}}{Dt} = \sum_{j\in liquid} \frac{2D_A m_j \overrightarrow{r_{ij}}}{\rho_j (\overrightarrow{r_{ij}})^2} (C_{A,i} - C_{A,j}) \nabla W_{ij}$$

$$+ \sum_{j\in liquid} \frac{m_j \overrightarrow{r_{ij}}}{\rho_j (\overrightarrow{r_{ij}})^2} \mu_{M^+} (C_{A,i} - C_{A,j})(\phi_i - \phi_j) \nabla W_{ij},$$

where subscript A refers to anion properties.

As the cations are reduced at the interface they will deposi

decrease in cation concentration at the interface. During charging, th

be balanced by the rate of gain of the solid (m_k) due to precipitation. T

via the discretization scheme of Tartakovsky *et al.*[44]

$$\frac{Dm_K}{Dt} = S_s \sum_{k\in liquid} \frac{m_k}{\rho_k} (\overrightarrow{n_k} + \overrightarrow{n_i})(\beta_k + \beta_i) \nabla W_{ik},$$

where the subscripts k and i represent solid and liquid particles respe

is twice the initial mass, the nearest fluid particle will precipitate and b

The governing equations are implemented into the SPH me

Large-scale Atomic/Molecular Massively Parallel Simulator (LAM

domain is discretized as 150 by 150 units of h, which is the smoothin

360,000 discrete SPH particles with a particle density of 30 particles

utilized to approximate the sharp boundary at the reactive interface a

been verified. To do so, both the radius growth equation and the nu

simplified, isolated, and then compared to their analytical solutions.

For both verification cases, the system does not model pl

constant concentration boundary condition at the anode-electrol

These simplifications allow the specified equation to be solved for an

verification case is the radial growth equation. Here the system is ass

flat surface, i.e. no nuclei present, where the curvature, k, is equal to

and further Eq. (9), to the traditional Butler-Volmer equation without

$$\frac{dr}{dt} = i_0 V_m [\exp\left(\frac{\alpha_a F}{RT}\eta\right) - \exp\left(\frac{\alpha_c F}{RT}\eta\right)]$$

This simplification allows us to solve the radius equation abo

solution for the radius of nuclei at a particular time ($r(t)$).

$$r(t) = r_0 + i_0 V_m \left[\exp\left(\frac{\alpha_a F}{RT}\eta\right) - \exp\left(-\frac{\alpha_c F}{RT}\eta\right.\right.$$

The initial nuclei radius, which must be larger than t

thermodynamically favorable to grow is given by r_0 and t is the

nucleates was obtained from the numerical data and compared direct

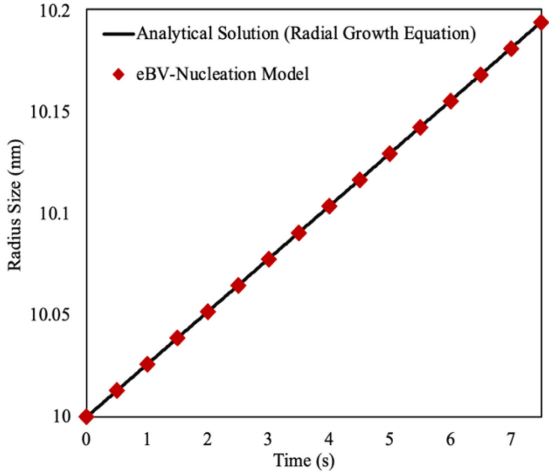

Figure 1: Comparison of numerical solution to ana
solution for radial growth equation.

The second verification case is the verification of the nucleatio

concentration condition is assumed and the resulting equation for

given as,

$$\frac{dn(\vec{r_s},t)}{dt} = N\frac{\omega_c}{g_c}\left(\frac{\Delta G_c}{3\pi k_B T}\right)^{1/2} exp\left(-\frac{\Delta G_c}{k_B T}\right)$$

Where N is defined as $N = N_A C_{Li^+} d$ and is a constant value. This simp

for the analytical solution, assuming that there are, initially, no nuclea

The final verification compares the numerical result to the

system undergoes changes in surface energy. To obtain the data from

the surface energy was varied over multiple simulations. The steady

then extracted from the simulation data and plotted against Eq. (22)

surface energy increases, the steady-state nucleation rate decreases.

well with the analytical solution with an average error of less than 5%

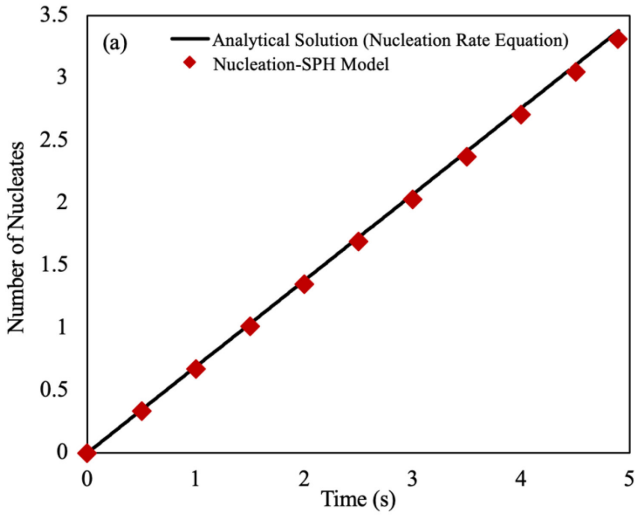

Figure 2: Comparison of numerical solution to analytical solution for the stead
comparison with respect to a change in time over five seconds of simulation time (
change in surface energy

2.3 Density Functional Theory Calculations:

valence electrons for Li, Al, C, N, O, F, and P, respectively. Calculatio
planewave energy cut off 450 eV, Pulay density mixing [54,55] with
and a Marzari-Vanderbilt smearing of occupations [56] (cold smearing

Starting structures were obtained from the Materials Project
154, mp-12957, mp-1067793, and mp-157) and re-optimized within
the BFGS and MDMin algorithms as implemented in ASE. Subsequent
Li(100) surface was constructed using ASE and its structure re-optimiz
at the bulk values. To study substitutional defects (Al, C, N, O, F, P)
Li(100) was created, where n = 3 ,5, 7 and two Li atoms on oppos
replaced by defect atoms. Both faces contain a defect to prevent t
dipole along the perpendicular direction due to the presence of the de
were placed in the center of the top and bottom faces of the supercell
structure was optimized while the lattice constants were kept to t
structural optimizations, forces on atoms were converged to less than

The surface energy was calculated as:

E

pseudoconvex energy surfaces. The MDMin-optimized geometries a

our presented results using the BFGS algorithm. The final surfa

presented in Table 1. These values are incorporated into our nucleat

14.

Table 1: DFT-Predicted surface energies for a series of defects at diffe
sake of analysis, the electronegativity associated with the defect is sh

Defect Type	**Concentration** ($10^{18}\ defects\ cm^{-2}$)	**Electronegativi**
Pristine Li	-	1
Carbon Substitutional	1.0632 2.9536 5.7888	2.5
Phosphorus Substitutional	1.0632 2.9536 5.7888	2.1
Fluorine Substitutional	1.0632 2.9536 5.7888	4
Aluminum Substitutional	1.0632 2.9536 5.7888	1.61
Oxygen Substitutional	1.0632 2.9536 5.7888	3.44
Nitrogen Substitutional	1.0632 2.9536	3.04

The simulation domain is comprised of an anode, a layer adja

the diffusion layer, where transport occurs, and the dendrite str

contains a constant concentration region, a distance L from the anod

simulation domain prior to dendrite growth. As the simulation progre

occurs the reactive boundary will adapt to the newly formed dend

presented in Section 2 is a universal model, thus cations and anions v

respectively. However, for the remainder of the study the cations w

the application of the method to dendrite growth and electrodeposit

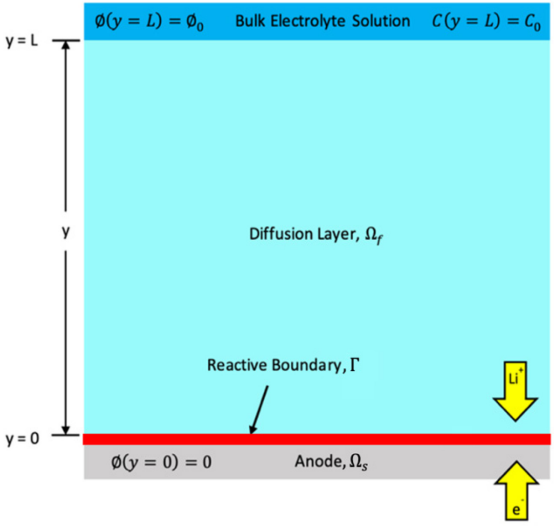

Figure 3: Schematic of the simulation domain including anode surface (Ω_s grey

$$C_i(y = L, t) = C_{i,L}$$

The Li^+ and anion concentrations are equal and constant in

electroneutrality is assumed at this location,

$$z_{Li^+}C_{Li^+} + z_A C_A = 0$$

$$\nabla C_i = 0$$

where z_{Li^+} and z_A are the charge of the Li^+ and anions, respectivel

concentration. There is no initial concentration gradient for Li^+ or ani

The potential at the reactive boundary, Γ, is the reference po

ground potential.

$$\phi(\vec{r_s}, t) = 0, \vec{r_s} \in \Gamma, t > 0$$

A constant voltage is applied to the top boundary at the cons

resulting in a fixed potential, ϕ_0, relative to the reference potential.

$$\phi(y = L, t) = \phi(\vec{r_f}, t), t > 0$$

Upon the application of this charging voltage, the anions will

while the Li^+ will travel toward the anode. This results in a buildup o

Here the Li^+ will react with electrons (e^-) and deposit as solid lithium

that is observed experimentally[16]. For example, because the diffu

down by approximately two orders of magnitude, the diffusion coeffi

same proportion to maintain equivalent ratios between the diffusi

diffusion coefficient. The physical properties used throughout this w

2.

Table 2: Simulation Parameters

Parameter	Symbol	Va
SPH particle interval	Δx	0.0
Kernel Density [12]	n_{eq}	
Diffusion coefficient* [7,13,60]	D	1
Mobility [12]	μ	0
Anion and Cation concentration (Initial) [61]	$C_{A,0}/C_{Li^+,0}$	0
Anion and Cation concentration (Bulk Electrolyte) [61]	$C_{A,L}/C_{Li^+,L}$	0
Transfer coefficients [32]	α_A, α_C	0
Reaction Rate* [10]	k^0	1.0
Applied potential	$\emptyset_{APP}$	

* Adjusted parameter to minimize computational time while preserving the physics of the system.

3.1 Qualitative Experimental Comparisons:

The model's ability to accurately represent a physical syst

comparison to experimental data. A limitation of experimentally vali

properties in comparison to a bare Li anode as determined via DFT c

was observed that the plating on the high energy Li-Sr anode was si

dendritic (Fig. 4a) than that on the low energy pristine Li anode (Fig. 4

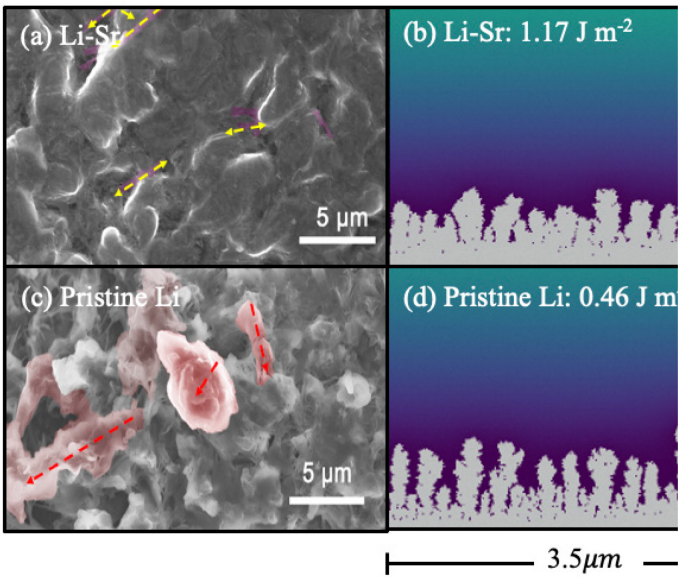

Figure 4: Dendrite comparison of different anodes after cycling. (a) Top-view SEM of Li-S
Sr anode with high interfacial energy (c) Top-view SEM of Pristine Li anode (d) model pr
low interfacial energy. Adapted with permission from S. Liu, X. Ji, J. Yue, S. Hou, P. Wan
Han, J. Tu, C. Wang, High Interfacial-Energy Interphase Promoting Safe Lithium Metal Bat
2438–2447. https://doi.org/10.1021/jacs.9b11750**.** Copyright 2020 American Chemical S

To compare the model results to that of the experimental res

flat morphologies minimize surface area and decrease the rate of reac

being consumed at the interface, the system remains reaction-limit

mossy morphology as seen in Fig. 4b. These predictions compare

reported in Liu *et al.*[17].

Based on the case presented above, as well as additional

increased surface energy leads to a more favorable nucleate morphol

rates resulting in a "layered" deposition as opposed to an "island

concluded that the computational model presented in this paper is

physical system.

4. Effect of Surface Energies and Transport on Dendrite Growth:

The nucleation-SPH model presented throughout this paper, in

used to investigate how defects in the lattice of the anode impact th

anode-electrolyte interface. It is nearly impossible to have a Li metal a

any lattice defects including impurity atoms and vacancies [14,15]. T

study how these defects impact the stability of the anode-electro

performance. To do this, seven different anodes with varying types an

affected by this increase. For most defect types including C, N, Al, an

positive increase in surface energy as the concentration of defect

surface formation is less favorable with increase of defect-defect inte

is a negative relationship between concentration and surface energy

may be related to the relative higher electronegativity of F and O, wh

a net negative charge on the defect, localizing the electron density. Th

have very little effect on the surface energy in comparison to pristine

metallic system; however, the surface energy was still directly propor

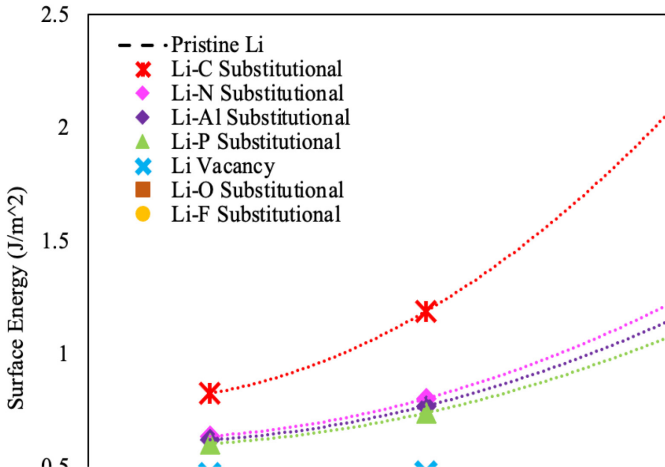

The surface energies were then implemented into the nucleat

how dendrite growth was impacted by these defects. Fig. 6 shows den

for selected defects at a concentration of 2.9536(10^{18}) $defects\ cm^{-2}$

seen in Fig. 6b for a pristine Li anode with a surface energy of 0.46

growth across the surface. This unstable plating is due to the low su

Li anode. When impurity atoms are present that cause an increase in

the growth across the anode is significantly denser (Fig. 6c and d). Th

surface energy creates a large energy barrier for nucleation and gr

Because of this large energy barrier, the rate at which the system fo

the nucleates are larger with smaller surface curvatures resulting in r

a smaller reaction flux at the anode-electrolyte interface[23,25]. Thu

the interface results in the system remaining in a reaction-limited reg

denser growth. This improvement in plating stability can be seen the

are present in the anode (Fig. 6d) because it creates the highest ener

atoms such as F are present in the crystal lattice, the surface ener

significantly more branched growth (Fig. 6a). This is due to fast nucl

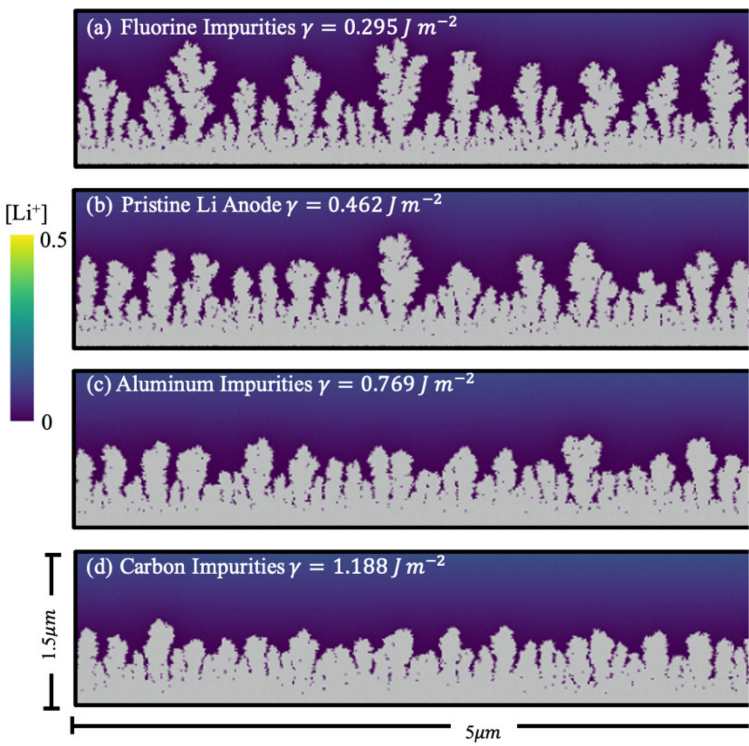

Figure 6: Model prediction of dendrite growth on Li anodes with varying defect typ
Li anode (b) 2.9536(10^{18}) $defects\ cm^{-2}$ Aluminum Impurity atoms (c) 2.9536(10^{1}
atoms (d) 2.9536(10^{18}) $defects\ cm^{-2}$ Fluorine impurity atoms. The color scheme
for Li^{+} and the solid particles are colored grey for visualization.

To further explain these growth regimes, we can visualize the

by isolating the effect that surface energy has on the reaction. In the

potential was kept constant between cases so that the effect of surfa

larger reaction at the interface due to increased reaction sites and

This results in the rapid consumption of Li^+ that outweighs the trans

leading to the highly negative flux observed at the tips of the dendrite

these conditions, the system exists in a transport-limited regime and t

the tips of the dendrites before reacting resulting in the branched gro

in Fig. 7b[63].

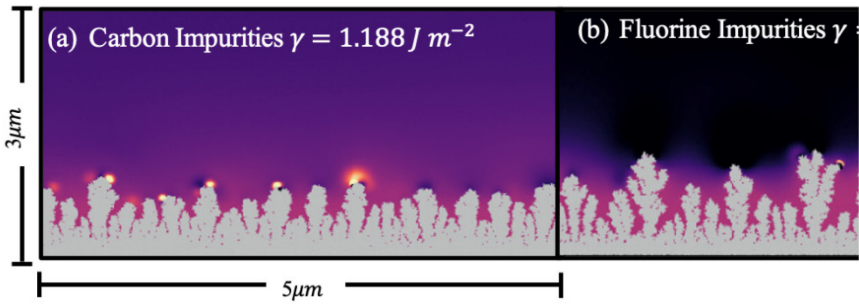

Figure 7: Model prediction of Li dendrite growth on (a) Surface with carbon im
and (b) surface with Fluorine impurities and a low surface energy. The Li^+ flux
are colored gray to distinguish them from the electrolyte.

In addition to how the type of defect impacts Li plating, the ef

of these defects has on plating was also studied. Fig. 8 shows the

energy surface with the smaller amount of F impurity atoms results

dendrites (Fig. 8d) than the surface with the higher concentration of

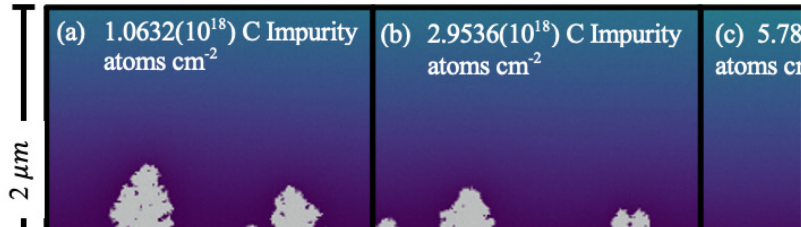

Figure 8: Predicted dendrite growth on surfaces with varying concentration
1.0632(10^{18}) C Impurity atoms cm^{-2} (b) 2.9536(10^{18}) C Impurity atoms cm^{-2} (c) 5.788
1.0632(10^{18}) F Impurity atoms cm^{-2} (e) 2.9563(10^{18}) F Impurity atoms cm^{-2}

While F impurities in the Li metal anode led to smaller inte

(001) produces significantly larger and more branched dendritic str

pristine Li anode (Fig. 9b) due to its low interfacial energy. Conversely

(111) results in a suppression of dendrite growth and denser structur

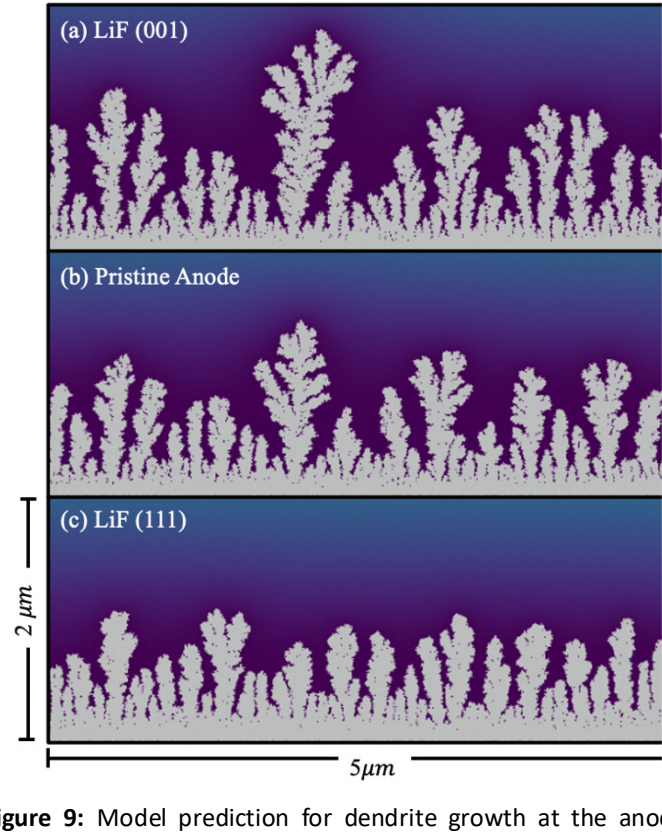

Figure 9: Model prediction for dendrite growth at the anod

comparing different SEI components with the pristine Li anod

LiF (001), *0.35* $J\ m^{-2}$ (b) pristine Li anode, *0.462* $J\ m^{-2}$ and (c) L

$J\ m^{-2}$.

dendrite growth for the anode surface utilizing the surface energy

varying diffusion coefficients. The LiF (001) surface energy was chos

impact that transport properties play on Li deposition under the e

energy surface. Fig. 10a shows the dendrite growth when the diffusion

to the baseline diffusion coefficient, D_0. Fig. 10b through c show t

coefficient near the interface increases from twice the base-line diffus

that of the base-line diffusion. When the diffusion coefficient incre

dendrites become denser. However, there are still clear dendritic st

interface. As the diffusion coefficient increases to $5D_0$ (Fig. 10c) and fu

plating becomes homogenous, and a moss-like morphology is ob

remaining in a reaction limited regime as opposed to the transport

Fig. 10a. These simulations were compared at an equivalent state-o

mass of Li deposited.

The increased plating stability observed experimentally, wh

present, is not due to the interfacial energy alone. Instead, for LiF

energy is low, it is dominated by the improved transport of Li^+ at th

dendrite growth and a moss-like morphology. While F substitutional d

in decreased interfacial energy and problematic dendrite growth (Fig.

or question the improved performance seen with an LiF-rich SEI la

results indicate the significance of both nucleation and growth in un

how the interplay between various physics (i.e. Li+ transport vs. sur

the suppression of dendrites and a more homogenous plating.

5. Conclusions

A novel dendrite growth model that captures the nucleat

electrolyte interface through the expansion of a previous mo

transport[11,13], a spatially and temporally varying electric fie

kinetics[10] was presented. To capture nucleation physics, a radial g

hemispherical nucleate as well as a steady-state nucleation rate v

the accuracy of the model. In addition, the ability of the model to r
was evaluated through qualitative comparison to experimental re
interfacial energy surface led to decreased nucleation and a suppr
[17,21–26]. The morphology of the dendrites predicted by the nuclea
well with the experimental results for both the high and low surface e

The model was then coupled with DFT calculations to evaluat
as impurity atoms, and the concentration of these defects impacted i
used to calculate the surface energy for the Li anode when specific im
and Al) and vacancies were present. These energies were then comp
Li metal anode. The results show that when certain impurity atoms
surface energy increases while other impurities such as F decreas
vacancies show very little deviation from the pristine anode. Ad
between the concentration of impurity atoms and surface energy w
atoms with smaller electronegativities (N, C, P, Al) surface energy and
directly proportional meaning that as the concentration of impur
energy increases. Conversely, for high electronegativity atoms such

surface. When C impurity atoms were present, the surface energy inc

suppression in the dendrite growth was observed. Finally, the surface

the lowest surface energy (0.294 J m^{-2}) resulting in extensive dendrit

In addition to the type of defect present, the concentration of defec

F, as the concentration of defect atoms increased, the surface energy

branched and problematic dendrites. C impurity atoms had the oppos

the concentration of impurity atoms of C increased, the surface e

resulted in significant improvement to the homogeneity of Li plating a

across the interface.

Based on the predicted results from the nucleation-SPH mod

experimental results it can be concluded that higher surface energy s

more stable Li plating[16,17,21–26]. Additionally, this work shows th

metal anode such as C can greatly improve the deposition wherea

instability. Further, a higher concentration of beneficial atoms will lea

across the anode due to the direct proportionality between concen

and the large energy barrier for the system to overcome to form

specified surface facets resulting in more growth, when considering

consider the impact it has on Li^+ transport near the anode. It was show

transport effects as well as the interfacial energies, an LiF-rich SEI laye

transport, a suppression of dendritic growth, and a more stable inter

In this work, we consider the impact that interfacial en

morphology by decoupling the interfacial energy from other physical a

allowing us to compare each case under equivalent conditions. Whil

regarding the impact of interfacial energies under the conditions tha

is important to note that this does not negate the importance of c

parameters such as charging conditions, transport properties, an

example, while the trends presented exist under our specific condit

applied to the system the impact that interfacial energy has on the r

influential. Thus, while computational models like the one presented

insight into the physics occurring and how they are influenced by indiv

the system in its entirety through the combination of computation ar

critical to the commercialization of lithium metal batteries.

Research Science and Engineering Center program through the UC Irvi

Active Materials (DMR-2011967). Additional support was provided

Computing and Computational Science and Engineering at Boston

Focused Research Program. We would like to acknowledge com

Advanced Cyberinfrastructure Coordination Ecosystem: Services & S

supported by the NSF grant number ACI-1548562, the National

Computing Center (NERSC), a DOE Office of Science User Facility s

Science of the U.S. Department of Energy under Contract No. DE-AC

University's Research Computing Services.

Author Declarations

Conflict of Interest

The authors have no conflict to disclose.

Data Availability

Data on dendrite growth and morphology were obtained via

code base modified for SPH and our system. The SPH data that suppo

and the codes used to obtain the data are

(https://github.com/emilymryan/LAMMPS-Dendrite-Nucleation-and-

D_i	diffusion coefficient, $\mu m^2\ s^{-1}$
e^-	electrons
$E_{BulkofDefect}$	energy per atom of a chunk of defect atoms, J
E_{defect}	energy of Li slab of a specific number of defected ato
E_{surf}	slab surface energy, J
F	Faraday constant, $C\ mol^{-1}$
g_c	number of atoms in the critical nucleus
ΔG	formation energy of critical nucleus, J
h	smoothing length, μm
i_0	exchange current density, $A\ \mu m^{-2}$
k	curvature, μm^{-1}
k^0	reaction rate constant, $\mu m\ s^{-1}$
K_B	Boltzmann constant, $J\ K^{-1}$
Li_+	lithium ions
m	mass of an individual particle, μg
M^+	cations
n	number of nucleates in the system
$\vec{n}$	normal vector
N	total number of atoms per unit surface area
N_A	Avogadro's number, μmol^{-1}
r	radius of nuclei, μm
r_{eq}^*	critical nuclei radius, μm
$\vec{r_f}$	location in the liquid domain (diffusion layer)
$\vec{r_{ij}}$	distance between particles, μm
$\vec{r_s}$	location in the solid domain (anode and dendrites)
r_0	initial nuclei radius
R	ideal gas constant, $J\ mol^{-1}\ K^{-1}$
S_c	surface area of nucleate exposed to the electrolyte,
S_n	flux for a single hemispherical nucleate, $\mu mol\ \mu L^{-1}$ s
S_s	total flux in system, $\mu mol\ \mu L^{-1}\ s^{-1}$
t	time, s

η	overpotential, V
Θ	contact angle
μ_i	migration coefficient, $\mu\mathrm{m}^2\ \mathrm{V}^{-1}\ \mathrm{s}^{-1}$
ρ	density of a particle, $\mu\mathrm{g}\ \mu\mathrm{m}^{-3}$
ρ_{charge}	net charge density, $\mathrm{C}\ \mu\mathrm{m}^{-3}$
$\emptyset_{App}$	applied potential, V
$\emptyset_{eq}$	equilibrium potential, V
ω_c	frequency of collision of cations with critical nuclei, s
Ω_f	fluid domain (diffusion layer)
Ω_s	Solid domain (anode and dendrites)

Abbreviations

Al	aluminum
C	carbon
CNT	classical nucleation theory
CSR	continuum surface reaction
Cu	copper
DFT	density functional theory
F	fluorine
LAMMPS	large-scale atomic/molecular massively parallel simu
Li	lithium
N	nitrogen
ND	nanodiamond
O	oxygen
P	phosphorus
PAW	projector-augmented wave
P2D	pseudo two-dimensional
SEI	solid-electrolyte interphase layer
SPH	smoothed particle hydrodynamics

References:

[1] B. Liu, J.G. Zhang, W. Xu, Advancing Lithium Metal Batteries, Jo
https://doi.org/10.1016/j.joule.2018.03.008.

[2] P.G. Bruce, S.A. Freunberger, L.J. Hardwick, J.M. Tarascon, LigO
high energy storage, Nat Mater 11 (2012) 19–29. https://doi.o

[3] X. Zhang, Y. Yang, Z. Zhou, Towards practical lithium-metal ano
(2020) 3040–3071. https://doi.org/10.1039/c9cs00838a.

[4] L. Frenck, G.K. Sethi, J.A. Maslyn, N.P. Balsara, Factors That Con
Dendrites and Other Morphologies on Lithium Metal Anodes, F
https://doi.org/10.3389/fenrg.2019.00115.

[5] M.P. Bondarde, R. Jain, J.S. Sohn, K.D. Lokhande, M.A. Bhakare
Carbon-based anode materials for lithium-ion batteries, Lithiu
521–545. https://doi.org/10.1016/B978-0-323-91934-0.00004-

[6] X. Guan, A. Wang, S. Liu, G. Li, F. Liang, Y.W. Yang, X. Liu, J. Luo
Lithium Metal Anodes, Small 14 (2018). https://doi.org/10.100

[7] J. Tan, A.M. Tartakovsky, K. Ferris, E.M. Ryan, Investigating the
Mass Transport on Dendrite Growth in High Energy Density Lit
Electrochem Soc 163 (2016) A318–A327. https://doi.org/10.11

[8] D. Sharon, P. Bennington, S.N. Patel, P.F. Nealey, Stabilizing de
by limiting spatial dimensions in nanostructured electrolytes, A
2889–2896. https://doi.org/10.1021/acsenergylett.0c01543.

[9] T. Melsheimer, M. Morey, A. Cannon, E. Ryan, Modeling the ef
dendrite growth in lithium metal batteries, Electrochim Acta 43
https://doi.org/10.1016/j.electacta.2022.141227.

[10] M. Morey, J. Loftus, A. Cannon, E. Ryan, Interfacial studies on t
anodes for guided lithium deposition in lithium metal batteries
Physics 156 (2022). https://doi.org/10.1063/5.0073358.

[11] A. Cannon, E.M. Ryan, Characterizing the Microstructure of Sep
Batteries and Their Effects on Dendritic Growth, ACS Appl Ener
7861. https://doi.org/10.1021/acsaem.1c00144.

X-ray Microtomography, ACS Energy Lett 7 (2022) 1120–1124. https://doi.org/10.1021/acsenergylett.2c00255.
[16] X.B. Cheng, M.Q. Zhao, C. Chen, A. Pentecost, K. Maleski, T. Ma J. Jiang, Y. Gogotsi, Nanodiamonds suppress the growth of lithi Commun 8 (2017). https://doi.org/10.1038/s41467-017-00519
[17] S. Liu, X. Ji, J. Yue, S. Hou, P. Wang, C. Cui, J. Chen, B. Shao, J. Li High Interfacial-Energy Interphase Promoting Safe Lithium Me Soc 142 (2020) 2438–2447. https://doi.org/10.1021/jacs.9b117
[18] A. Ramasubramanian, V. Yurkiv, T. Foroozan, M. Ragone, R. Sha Mashayek, Lithium Diffusion Mechanism through Solid-Electro Rechargeable Lithium Batteries, Journal of Physical Chemistry 10245. https://doi.org/10.1021/acs.jpcc.9b00436.
[19] L. Qian, Y. Zheng, T. Or, H.W. Park, R. Gao, M. Park, Q. Ma, D. L Advanced Material Engineering to Tailor Nucleation and Growt Deposition for Anode-Less Lithium Metal Batteries, Small 18 (2 https://doi.org/10.1002/smll.202205233.
[20] C.P. Yang, Y.X. Yin, S.F. Zhang, N.W. Li, Y.G. Guo, Accommodati collectors with a submicron skeleton towards long-life lithium Commun 6 (2015). https://doi.org/10.1038/ncomms9058.
[21] A. Pei, G. Zheng, F. Shi, Y. Li, Y. Cui, Nanoscale Nucleation and Electrodeposited Lithium Metal, Nano Lett 17 (2017) 1132–113 https://doi.org/10.1021/acs.nanolett.6b04755.
[22] J. Lopez, A. Pei, J.Y. Oh, G.J.N. Wang, Y. Cui, Z. Bao, Effects of P Electrodeposited Lithium Metal, J Am Chem Soc 140 (2018) 11 https://doi.org/10.1021/jacs.8b06047.
[23] K.Y. Cho, S. Cho, G.Y. Jung, K.S. Eom, Metal shields with crystal incorporated into integrated architectures for stable lithium m Environ Sci (2024). https://doi.org/10.1039/d3ee02372a.
[24] D.T. Boyle, S.C. Kim, S.T. Oyakhire, R.A. Vilá, Z. Huang, P. Sayav Correlating Kinetics to Cyclability Reveals Thermodynamic Orig Morphology in Liquid Electrolytes, J Am Chem Soc 144 (2022) 2

[29] E. Maeda, R.S. Welch, C.J. Wilkinson, J.C. Mauro, Atomistic mo
nucleation in anorthite-based glasses, J Non Cryst Solids 615 (2
https://doi.org/10.1016/j.jnoncrysol.2023.122411.
[30] P. Jreidini, G. Kocher, N. Provatas, Classical nucleation theory i
model, Phys Rev E 97 (2018). https://doi.org/10.1103/PhysRev
[31] D.R. Ely, R.E. García, Heterogeneous Nucleation and Growth of
on Negative Electrodes, J Electrochem Soc 160 (2013) A662–A6
https://doi.org/10.1149/1.057304jes.
[32] C. Monroe, J. Newman, Dendrite Growth in Lithium/Polymer S
150 (2003) A1377. https://doi.org/10.1149/1.1606686.
[33] K.S. Nagy, S. Kazemiabnavi, K. Thornton, D.J. Siegel, Thermodyn
Nucleation Rates for Electrodeposition on Metal Anodes, ACS A
(2019) 7954–7964. https://doi.org/10.1021/acsami.8b19787.
[34] E.M. Ryan, K. Ferris, A. Tartakovsky, M. Khaleel, Computationa
Limitations in Li-Air Batteries, ECS Trans 45 (2013) 123–136.
https://doi.org/10.1149/04529.0123ecst.
[35] J. Tan, E.M. Ryan, Numerical Modeling of Dendrite Growth in a
System, ECS Trans 53 (2013) 35–43. https://doi.org/10.1149/05
[36] X. Shan, M. Morey, Z. Li, S. Zhao, S. Song, Z. Xiao, H. Feng, S. Ga
Ryan, K. Xu, M. Tian, Y. He, H. Yang, P.F. Cao, A Polymer Electro
Transport Number for Safe and Stable Solid Li-Metal Batteries,
4342–4351. https://doi.org/10.1021/acsenergylett.2c02349.
[37] J. Tan, A.M. Tartakovsky, K. Ferris, E.M. Ryan, Investigating the
Mass Transport on Dendrite Growth in High Energy Density Lit
Electrochem Soc 163 (2016) A318–A327. https://doi.org/10.11
[38] Y.D. Gamburg, G. Zangari, Theory and Practice of Metal Electro
York, 2011. https://doi.org/10.1007/978-1-4419-9669-5.
[39] J. Newman, Thomas-Alyea Karen, ELECTROCHEMICAL SYSTEMS
[40] D.R. Ely, R.E. García, Heterogeneous Nucleation and Growth of
on Negative Electrodes, J Electrochem Soc 160 (2013) A662–A6
https://doi.org/10.1149/1.057304jes.

[45] E.M. Ryan, A.M. Tartakovsky, C. Amon, A novel method for mo
Robin boundary conditions in smoothed particle hydrodynami
181 (2010) 2008–2023. https://doi.org/10.1016/j.cpc.2010.08.
[46] I.J. Schoenberg, Contributions to the Problem of Approximatio
Analytic Functions, in: C. de Boor, ed. Birkhauser (Eds.), I. J. Sch
Birkhäuser Boston, Boston, MA, 1988: pp. 3–57. https://doi.org
0433-1_1.
[47] A.P. Thompson, H.M. Aktulga, R. Berger, D.S. Bolintineanu, W.
in ’t Veld, A. Kohlmeyer, S.G. Moore, T.D. Nguyen, R. Shan, M.J
Trott, S.J. Plimpton, LAMMPS - a flexible simulation tool for pa
modeling at the atomic, meso, and continuum scales, Comput
https://doi.org/10.1016/j.cpc.2021.108171.
[48] J.J. Mortensen, A.H. Larsen, M. Kuisma, A. V. Ivanov, A. Taghiza
Haldar, A.O. Dohn, C. Schäfer, E.Ö. Jónsson, E.D. Hermes, F.A.
Levi, H. Jónsson, H. Häkkinen, J. Fojt, J. Kangsabanik, J. Sødequ
J. Enkovaara, K.T. Winther, M. Dulak, M.M. Melander, M. Oves
Walter, M. Gjerding, O. Lopez-Acevedo, P. Erhart, R. Warmbier
Kaappa, S. Latini, T.M. Boland, T. Bligaard, T. Skovhus, T. Susi,
Chen, Y.L.A. Schmerwitz, J. Schiøtz, T. Olsen, K.W. Jacobsen, K.
Python package for electronic-structure calculations, (2023).
http://arxiv.org/abs/2310.14776.
[49] J.J. Mortensen, L.B. Hansen, K.W. Jacobsen, Real-space grid im
projector augmented wave method, Phys Rev B 71 (2005) 035
https://doi.org/10.1103/PhysRevB.71.035109.
[50] J.P. Perdew, K. Burke, M. Ernzerhof, Generalized Gradient App
Phys Rev Lett 77 (1996) 3865–3868. https://doi.org/10.1103/P
[51] H.J. Monkhorst, J.D. Pack, Special points for Brillouin-zone inte
(1976) 5188–5192. https://doi.org/10.1103/PhysRevB.13.5188
[52] P.E. Blöchl, Projector augmented-wave method, Phys Rev B 50
https://doi.org/10.1103/PhysRevB.50.17953.
[53] C. Rostgaard, The Projector Augmented-wave Method, (2009).

[58] K. Nishikawa, M. Ota, S. Izuo, Y. Fukunaka, E. Kusaka, R. Ishii, J.
natural convection induced by electrodeposition of Li + ions or
cathode in propylene carbonate, Journal of Solid State Electroc
181. https://doi.org/10.1007/s10008-003-0447-z.
[59] J. Elezgaray, C. Léger, F. Argoul, Linear Stability Analysis of Uns
Electrodeposition in the Two-Dimensional Diffusion-Limited Re
145 (1998) 2016–2024. https://doi.org/10.1149/1.1838592.
[60] J. Tan, E.M. Ryan, Computational study of electro-convection e
in batteries, J Power Sources 323 (2016) 67–77.
https://doi.org/10.1016/j.jpowsour.2016.05.012.
[61] K. Nishikawa, T. Mori, T. Nishida, Y. Fukunaka, M. Rosso, Li den
mass transfer phenomenon, Journal of Electroanalytical Chemi
https://doi.org/10.1016/j.jelechem.2011.06.035.
[62] Y. Liu, X. Xu, M. Sadd, O.O. Kapitanova, V.A. Krivchenko, J. Ban,
Song, S. Xiong, A. Matic, Insight into the Critical Role of Exchan
Electrodeposition Behavior of Lithium Metal, Advanced Scienc
https://doi.org/10.1002/advs.202003301.
[63] P. Bai, J. Li, F.R. Brushett, M.Z. Bazant, Transition of lithium gro
electrolytes, Energy Environ Sci 9 (2016) 3221–3229.
https://doi.org/10.1039/c6ee01674j.
[64] S. Liu, X. Ji, J. Yue, S. Hou, P. Wang, C. Cui, J. Chen, B. Shao, J. Li
High Interfacial-Energy Interphase Promoting Safe Lithium Me
Soc 142 (2020) 2438–2447. https://doi.org/10.1021/jacs.9b117
[65] Y.X. Zhan, Z.Y. Liu, Y.Y. Geng, P. Shi, N. Yao, C. Bin Jin, B.Q. Li, G
Huang, Fluorinating solid electrolyte interphase by regulating p
interaction in lithium metal batteries, Energy Storage Mater 60
https://doi.org/10.1016/j.ensm.2023.102799.